

RSC Advances



This is an *Accepted Manuscript*, which has been through the Royal Society of Chemistry peer review process and has been accepted for publication.

Accepted Manuscripts are published online shortly after acceptance, before technical editing, formatting and proof reading. Using this free service, authors can make their results available to the community, in citable form, before we publish the edited article. This *Accepted Manuscript* will be replaced by the edited, formatted and paginated article as soon as this is available.

You can find more information about *Accepted Manuscripts* in the [Information for Authors](#).

Please note that technical editing may introduce minor changes to the text and/or graphics, which may alter content. The journal's standard [Terms & Conditions](#) and the [Ethical guidelines](#) still apply. In no event shall the Royal Society of Chemistry be held responsible for any errors or omissions in this *Accepted Manuscript* or any consequences arising from the use of any information it contains.

Cite this: DOI: 10.1039/c0xx00000x

www.rsc.org/xxxxxx

PAPER

Fabrication, mechanical properties, and biocompatibility of reduced graphene oxide-reinforced nanofiber mats

Lin Jin, *^a Dan Yue,^a Zhe-Wu Xu,^b Guobin Liang,^c Yilei Zhang,^d Jian-Fu Zhang,^a Xingcai Zhang,^e and Zhenling Wang*^a

5 Received (in XXX, XXX) Xth XXXXXXXXXX 20XX, Accepted Xth XXXXXXXXXX 20XX

DOI: 10.1039/b000000x

Fibrous functional scaffolds that could mimic cells' natural growth environment and govern cell-specific behaviors are crucial for meeting the requirements in tissue engineering. Graphene-based materials as an important one of them have captured researchers tremendous interests. However, few researches about graphene nanofibers with excellent electrical and mechanical properties have been
10 fabricated and found real application. In this study, we reported a novel PAN-reduced graphene oxide reinforced composite nanofiber mats (rGO-NFMs) which were fabricated by electrospinning process combining with chemical reduction. SEM, FTIR and XRD revealed that rGO-NFMs were successfully produced. These rGO-NFMs displayed superior mechanical properties (tensile strain and tensile stress are 18.5% and 1.38 MPa, respectively). The cell proliferation and morphology of adipose-derived stem cells (ADSCs as model cells)
15 biocompatibility, cell on the nanofibers formed stable cell-fiber constructs, and the rate of cell proliferation was similar to that of tissue culture plates (TCPs) and PAN nanofibers mats (PAN-NFMs). This study demonstrated that the rGO-NFMs maybe a good choice for application in the tissue engineering, particularly cell culture scaffold for electrical stimulation.

1. Introduction

As a star materials, graphene, verified to be a monolayer of
20 carbon atoms densely packed into a two-dimensional honeycomb crystal lattice, has recently sparked much research interest because of its unique properties such as the strongest mechanical strength and electrical conductivity.¹⁻¹¹ It has become the hot topic in the field of nanomaterials preparation due to its
25 outstanding potential applications. Advances have been achieved in the area of graphene-based polymer composite. Furthermore, previous study indicated that when it was incorporated in polymer, these properties of graphene manifest as remarkable improvements in the host material.¹²⁻¹⁴ For instance, graphene-based
30 polymer composites exhibited extraordinarily electrical property due to large conductivity and aspect ratio of the graphene sheets.^{15,16} On the other hand, the mechanical and thermal properties of these materials rank among the best in comparison with other carbon-based composites due to strong
35 interactions between polymer hosts and graphene sheets.^{16,17} Therefore, the highly conductive nature of graphene and the ease of incorporation into polymers have brought a new consideration to its potential applications in biomedical field, such as cell culture, controlled drug release, and biosensors.¹⁸⁻²¹

40 To date, different approaches were used to fabricate graphene-based composite nanomaterials, such as self-assembly technology, vacuum filtration and so on.²²⁻²⁴ However, these methods still need to overcome some crucial obstacles. For example, those graphene-based nanomaterials prepared using
45 above approach were difficult to scale up, as well as the architectural control for size and surface. On the other hand, they

can not effectively translate the properties of graphene into polymer. It is perhaps no surprise that researchers dedicate their enormous attention to developing novel preparation process for
50 overcoming the above drawbacks. Electrospinning is an exciting technique attracting more and more attention as a potential solution to the current challenges, which provides a simple and versatile technique for producing various nano-materials from a variety of polymers.²⁵⁻²⁸ Especially, the fabrication process is
55 time-saving and easy to scale up when compared with previously reported fabrication techniques for graphene nanomaterials.

Herein, we report a novel preparation approach of polyacrylonitrile (PAN)/reduced graphene oxide (rGO-NFMs) reinforced composite nanofiber mats for tissue engineering.
60 Firstly, GO and PAN were used to prepare GO composite nanofiber mats (GO-NFMs). Subsequently, chemical reduction process was employed to obtain graphene composite nanofiber mats. To evaluate the potential applications of this type of graphene composite nanofiber mats in tissue engineering,
65 adipose-derived stem cells (as model cells) were observed by assessing cellular attachment, proliferation, and morphology, and TCPs and PAN-NFMs were set as the control groups.

2. Results and discussion

2.1 Preparation of GO

70 It's well known that well exfoliated GO can form well-dispersed N,N-dimethyl-formamide (DMF) solution.²⁹ In this study, we prepared 5mg/mL GO and DMF solution by ultrasonication with a cell disrupter under 400 W of power for 30 min in 10 mL batches. GO sheets of the mixed solution were characterized by a

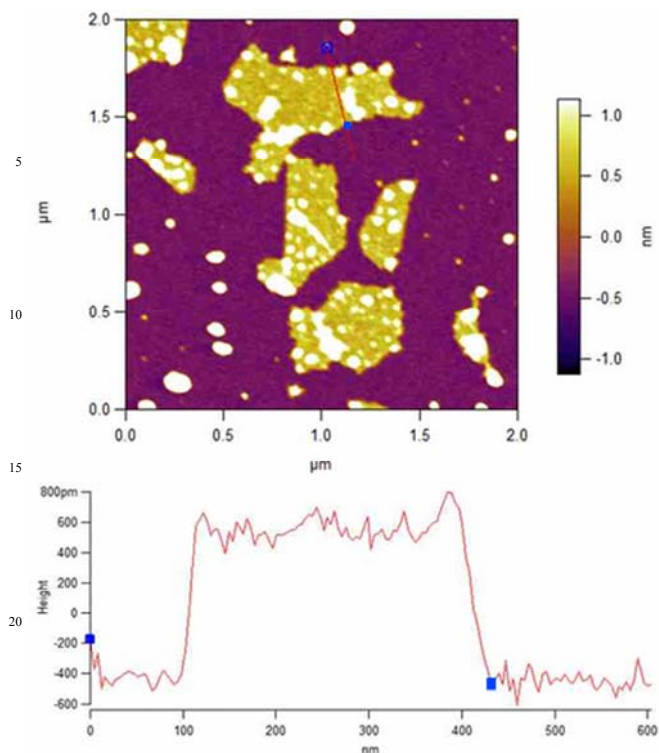


Fig. 1 AFM image and thickness of measured GO sheets.

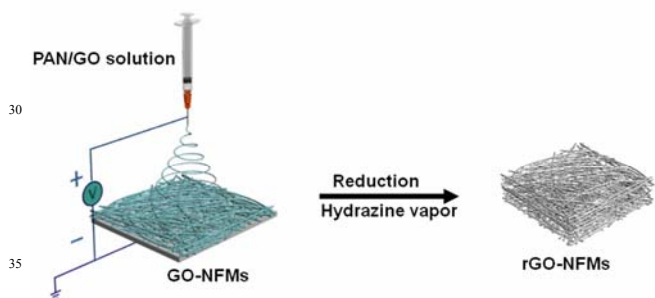


Fig. 2 Schematic illustration for fabrication of rGO-NFMs. The schematic includes of the fabrication of GO-NFMs by electrospinning technique and the formation of rGO-NFMs after reduction hydrazine vapor treatment.

tomic force microscopy (AFM) (as shown in Fig. 1), which offered immediate evidence for peeled-off single GO sheet. The original GO nanosheets were of irregular shape with uniform thickness and lateral dimensions ranging from tens to several hundred nanometers. The average thicknesses of the graphene oxide sheets is ~ 1.0 nm, which is much thicker than that of monolayer graphene oxide. As reported previously, these graphene oxide layers should be mostly monolayered, although these values are somewhat larger than the interlayer spacing (0.776 nm) of the parent GO. The experimental results indicated that we obtained well dispersion and size distribution monolayer GO solution.

2.2 Morphology and structure

Graphene-based nanocomposites with control of the size, shape, excellent physical and chemical properties, were often used to produce biosensors and cell culture scaffolds in biomedical field.

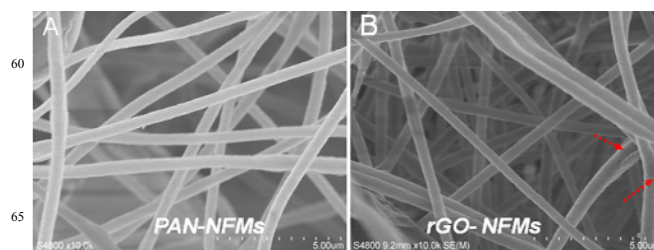


Fig. 3 SEM images of PAN-NFMs (A) and rGO-NFMs (B). The location denoted by red arrow is rGO sheets out of nanofibers.

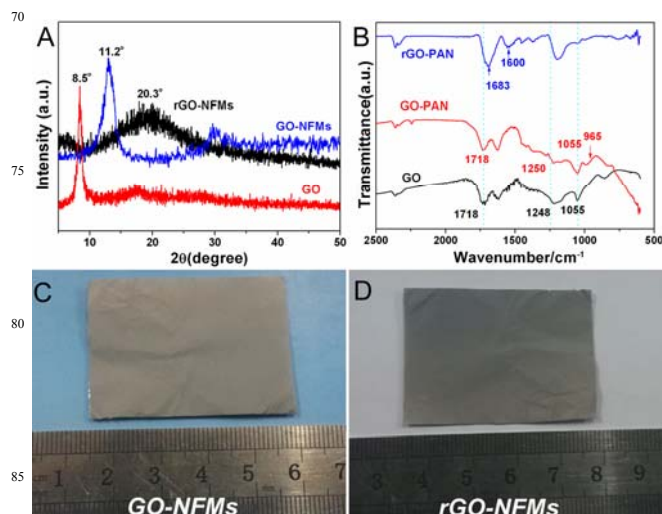


Fig. 4 XRD (A), FTIR (B) spectra of GO, GO-NFMs and rGO-NFMs. And optical photographs of (C) GO-NFMs, (D) rGO-NFMs.

In present work, the rGO-NFMs obtained by the electrospinning process combining with chemical reduction (the fabrication process was shown in Fig. 2), were characterized by SEM in order to determine the surface and diameter of nanofibers, and the presence of graphene dispersed in the matrix. Additionally, we also investigated the surface features of nanofibers in pure PAN nanofiber mats by SEM. As shown in Fig. 3, these two kinds of composite nanofibers exhibited a narrow diameter distribution (350 ± 30). In particular, several graphene sheets which were not completely embedded into the graphene composite nanofibers were observed, as denoted by red arrow in Fig. 3B. To further observe the surface morphology of the graphene nanofibers, high magnification SEM image was characterized, as shown in Fig. S1. It indicated that most of the graphene nanosheets were embedded into nanofibers. Despite the overall surface topograph of the composite nanofiber was still preserved, the roughness of the nanofibers surface was significantly increased. These results showed that suitable size distribution and amount of graphene did not change the integrated surface structure of the PAN nanofibers. Furthermore, we also can find that the structure of nanofibers was also well preserved before and after doping graphene, and graphene sheets well expand in nanofibers (as shown in Fig. S2). These results showed that graphene could successfully mix into the PAN nanofibers using electrospinning technology.

2.3 XRD analysis

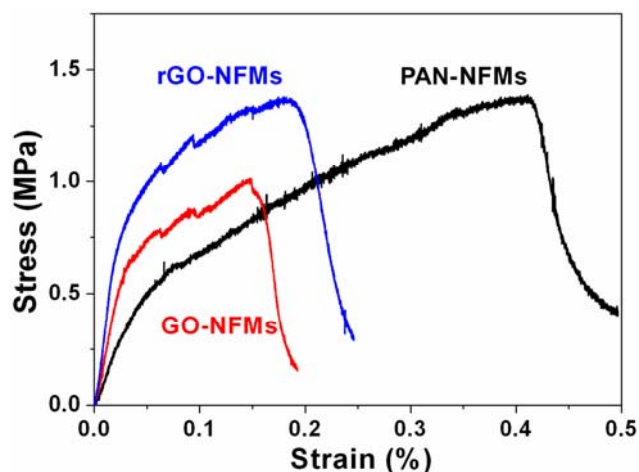


Figure 5. Mechanical tensile stress and tensile strain of NFM, GO-NFMs and rGO-NFMs, respectively.

Fig. 4A showed the X-ray diffraction (XRD) patterns of GO, GO-NFMs before and after the chemical reduction. As can be seen from the XRD patterns, GO reveals its characteristic peak at patterns, GO reveals its characteristic peak at $2\theta = 8.5^\circ$. After GO embedded into PNA nanofibers, a broad reflection with peak at $2\theta = 11.2^\circ$ was observed in GO-NFMs, which can be correlated to the interlayer distance of 0.87 nm in GO nanosheets. This value can be assigned to the (002) reflection peak.³⁰ After the chemical reduction, the large shift of (002) reflection peak changed from 11.2° to 20.3° , which was most likely due to the elimination of the oxygen-containing groups which resulted in lower d-spacing.

2.4 FTIR analysis

To gain further insights on GO-NFMs before and after reduction, we performed FTIR spectra measurements of them. FTIR spectra of GO, GO-NFMs and rGO-NFMs were shown in Fig. 4B. The GO spectrum reveals vibration band, corresponding to C=O stretching peak at 1718 cm^{-1} , C-OH (hydroxyl) stretching at 1248 cm^{-1} , and C-O stretching at 1055 cm^{-1} . In the spectrum of GO-NFMs, the GO characteristic peaks were clearly observed, and the peak at 965 cm^{-1} is attributed to the C-H of vinyl groups. These vibrational bands are visible evidences of successful formation of GO and PAN composite nanofibers. After chemical reduction, rGO-NFMs showed 1683 cm^{-1} characteristic peak of the vibration mode of adsorbed water molecules, and 1718 cm^{-1} and 1055 cm^{-1} characteristic peaks disappeared, and the peak at 1600 cm^{-1} corresponds to the C-H bond and the C=C, C=N stretching vibration, which indicated that the dominant oxygen-containing groups including -OH and C=O had almost been successfully removed completely.^{9, 30, 31} In addition, after the chemical reduction, the photographs showed that the color of GO composite nanofiber mats changed from yellow to black with weak metallic luster as shown in Fig. 4C and D. These results combined with the SEM images indicated that the reduced graphene composite nanofibers were successfully fabricated in our study.

2.5 Mechanical analysis

Mechanical properties were shown in Fig. 5, and the results dem-

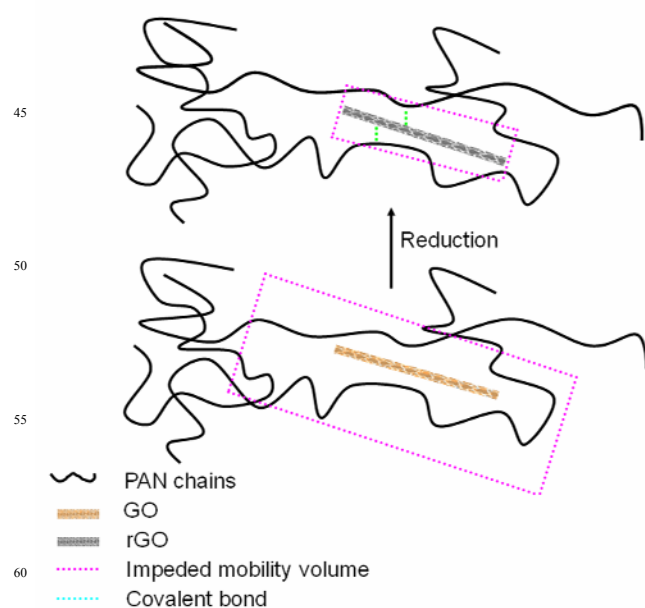


Figure 6. Schematic changes of the connection and mobility volume in the samples.

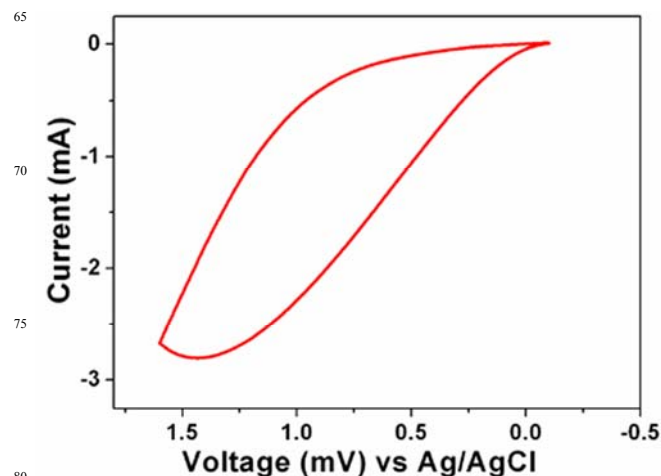


Fig. 7 Cyclic voltammetry of the rGO-NFMs.

onstrated that PAN-NFMs, GO-NFMs and rGO-NFMs exhibited typical plastic deformation under tensile loading at room temperature. Upon further straining, PAN-NFMs, GO-NFMs and rGO-NFMs showed typical fracture strengths of 1.36 MPa, 1.1 MPa and 1.38 MPa, at ultimate elongations of 40%, 25% and 18.5%, respectively. It can be seen that once the covalent incorporation of GO to PAN nanofibers, the fracture strength of PAN nanofibers has sharp decline, which is due to GO sheets generate a phase separation with PAN. Strikingly, the fracture strength of the reduced graphene oxide composite nanofiber mats has a significantly improved, while the breaking elongation became smaller compared to before reduction. This phenomenon could probably be attributed to rGO sheets providing maximal surface area for π - π stacking with polymer hosts and form close connection between rGO and PAN (green lines represent connection of covalent bond in Fig. 6). This connection made rG-

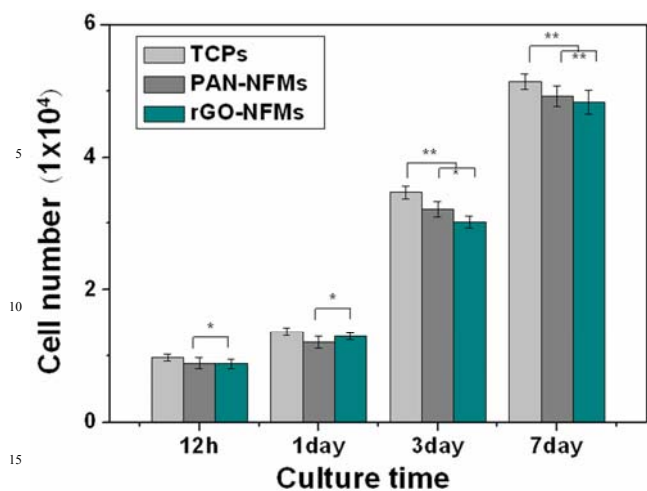


Fig. 8 The attachment and proliferation of ADSCs cultured on TCPs, PAN-NFMs and rGO-NFMs in various incubation periods by the PicoGreen dsDNA assay. ADSCs were originally seeded at 1.0×10^4 cells. Data are mean \pm SD, $N=3$, $*p < 0.05$, and $**p < 0.1$.

O have the ability to bind PAN and create a synergistic effect, and produce strong conjugations between the sheets of rGO and the adjacent polymer segments, which enhance the mechanical performance of nanofibers.⁹ On the other hand, the connections of rGO sheets and PAN chains also restrict the mobility volume of rGO sheets (red areas represent the mobility volume of rGO sheets in PAN-rGO composite nanofibers), which made the breaking elongation of rGO-NFMs decrease.³²

2.6 Electrochemical properties analysis

The electrochemical properties of the rGO-NFMs were characterized by measuring the cyclic voltammetry (CV). CV was performed using the rGO-NFMs as a working electrode and a platinum wire as a counter electrode against an Ag/AgCl reference electrode. rGO-NFMs with size of 2cm \times 2cm were immersed in PBS (PH=7.0), and the voltammograms were recorded at a scan rate of 50 mV/s. The CV can be seen in Fig. 7, which indicated that rGO-NFMs exhibited an order of magnitude higher charge carrying capacity for a given voltage and excellent conductivity. This is most likely due to the large surface of the rGO-NFMs, which hinders both the incorporation of dopant electronic into the matrix and the formation of tightly packed PAN chains that permit efficient electron transfer between polymer chains. In addition, these results showed that an appropriate range of current can be achieved to apply electrical stimulation for cells in culture (0.01-0.2mA).³³

2.7 Cytocompatibility

In this study, in order to evaluate the possibility of applying these rGO-NFMs in biotechnology, the ADSCs were cultured on the rGO-NFMs with a cell density 1.0×10^4 well for 7d period to examine the biocompatibility of rGO-NFMs, PAN-NFMs, and TCPs were set as the control groups. Cell attachment and proliferation on these mats were analyzed with Pico-Green dsDNA assay. As shown in Fig. 8, after 6h culture, ADSCs exhibited essentially similar cellular attachment: 97.5% ADSCs adhered o-

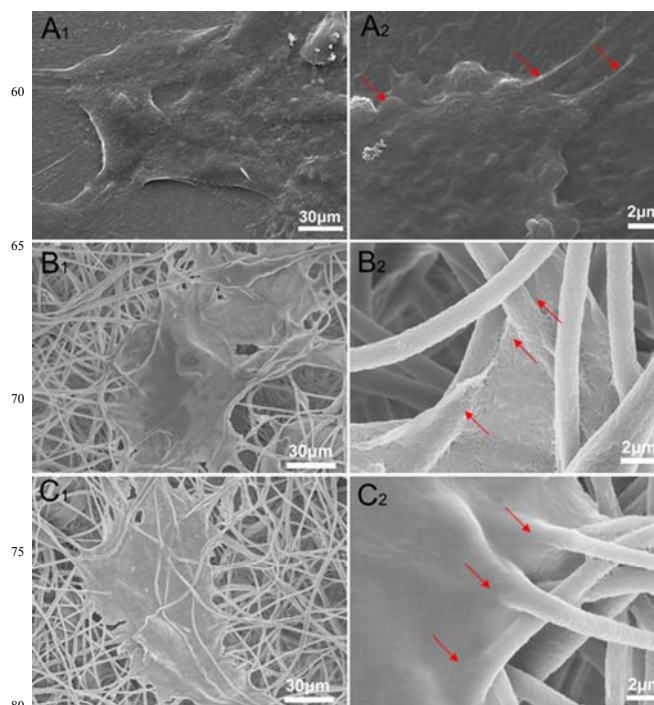


Fig. 9 SEM images of ADSCs cultured on TCPs (A₁, A₂), PAN-NFMs (B₁, B₂) and rGO-NFMs (C₁, C₂) for 3 days. Red arrows: pseudopods of ADSCs.

nto the TCPs, 88.9% ADSCs adhered onto the PAN-NFMs and 87.8% of the ADSCs adhered on the rGO-NFMs. During the culture period of 7 days, on day 1 and 3, the cell numbers on the rGO-NFMs were slightly less than that on the TCPs and PAN-NFMs. After 7 days culture, the number of cells on rGO-NFMs was up to 4.63×10^4 cells, the number of cells on PAN-NFMs and TCPs were 4.92×10^4 cells and 5.14×10^4 cells, respectively. These results strongly demonstrated that the rGO-NFMs promoted ADSCs proliferation and could provide a preferable cell survival microenvironment. The microscopic morphology of ADSCs cultured on the PAN-NFMs and rGO-NFMs was examined by SEM after 3 days culture. Fig. 9C₁-C₂ demonstrated that the morphology of the ADSCs cultured on the rGO-NFMs. These cells on rGO-NFMs spread widely along the graphene composite nanofibers, their abundant pseudopods adhered tightly to the nanofibers of rGO-NFMs and formed integrated cell-fiber constructs, and the cells in these constructs exhibited wide cell-cell and cell-nanofibers contact, which is helpful for the maintenance of cell activity. Moreover, the morphology of the ADSCs cultured on the PAN-NFMs were characterized, which were shown in Fig. 9B₁-B₂, cell also exhibited similar growth morphology as rGO-NFMs, spread widely along the PAN nanofibers, and formed cell-nanofibers constructs. While the ADSCs on TCPs also displayed a large number of cellular pseudopods, which spread randomly on the smooth surface of TCPs (as shown in Fig. 9A₁-A₂). These cellular morphological characteristics implied a positive interaction between ADSCs and nano-scale fibers of graphene composites and PAN nanofibers. These results indicated that the obtained rGO-NFMs could improve the cells activity obviously and impact the cells growth

morphology. Especially, nanofibers in the rGO-NFMs can be well guided cell growth along the nanofibers direction. Combined with excellent electrical conductivity and mechanical properties, their biocompatibility makes these rGO-NFMs be one of the most promising candidates in modern biotechnology applications, such as electroactive soft scaffolds for tissue engineering, drug delivery, cell culture and biosensors.

3. Experimental

3.1 Preparation of GO

GO was synthesized from natural graphite by a modified Hummers method as originally presented by Kovtyukhova and colleague.^{34, 35} GO was dispersed in DMF solution with 5mg/mL and the mixed solution was prepared under ultrasonication with a cell disrupter under 400 W of power for 30 min in 10 mL batches.

3.2 Fabrication of graphene composite nanofibers

The rGO-NFMs were fabricated by means of electrospinning technique combining with chemical reduction. Briefly, PAN (Mn=100k) was dissolved in above mixed solution of GO/ DMF at 10wt% under constant stirring until the mixture was clear, viscous, and homogenous. Subsequently, this PAN mixed solution was fed into a syringe capped with a 0.22 gauge blunt-tipped needle nozzle and driven by using a syringe pump (Silugao Co., Beijing, China) at a speed of 1.0 mL·h⁻¹. A voltage of 15 kV was supplied by a high DC power supply (Dongwen High Voltage, China) between the tip of the needle and the collector at a distance of 10 cm. The obtained GO-NFMs were collected by aluminum foil covered plastic plate, and then placed in vacuum for 2 days at room temperature to remove residual solvent. And then, these composite nanofiber mats were chemically reduced by hydrazine vapor at 90°C for 24h, followed by vacuum-drying at 80°C for 24 h.

3.3 Characterization of graphene composite nanofibers

The morphology of the rGO-NFMs was tested by using a scanning electron microscope (SEM, Hitachi S-3000N) at an acceleration voltage of 10 kV. The mechanical tensile stress-strain response of rGO-NFMs was evaluated using a micro-tensile testing machine (Sans-GB T528, ShenZhen, China). The chemical composition was examined by the FTIR spectroscopy (Bruker Co. Germany) and X-ray diffraction (XRD, RIGAKU Co., Japan). Electrical testing of rGO-NFMs were performed using an AutoLab PGstat and a 3-electrode system with PBS (pH = 7.0) as the electrolyte, a platinum wire as the counter electrode (CE), a saturated Ag/AgCl calomel electrode (SCE) as the reference electrode. Cyclic voltammetry (CV) was used to determine the charge capacity of the electrodes. The voltage was cycled from -0.1 to +1.55V vs. SCE at a rate of (50mV/s) while the current was measured.

3.4 In vitro cell seeding and culture

ADSCs were obtained from Chinese Academy of Medical Science and used to evaluate cell adhesion, proliferation and morphology on the rGO-NFMs. ADSCs were routinely cultivated in dulbecco's modified Eagle medium (DMEM, Thermo Fisher Scientific, USA) containing 10% (v/v) fetal bovine serum (FBS, Thermo Fisher Scientific, USA), 100 units/mL penicillin and 100

µg/mL streptomycin (Invitrogen, USA), at 37°C with 5% CO₂. The rGO-NFMs were cut into 6-well tissue culture plates by trimming with a sterile razor, sterilized by soaking in a solution of 70% ethanol and 30% PBS for 12 hours, followed by washing several times with PBS. ADSCs were seeded onto the mats and TCPs at a cell density of 1.0 × 10⁴ cell/well for cytocompatibility tests, Media was changed every two days.

Cell morphology was visualized using SEM. The cells were fixed with 3% glutaraldehyde for 2 hours and dehydrated using increasing ethanol/water concentrations (25%, 50%, 70%, 80%, 90%, 95% and absolute ethanol for 30 minutes each), subsequently dried by CO₂ critical point drying (Hitachi HCP-2) and sputter-coated with platinum before viewing under the SEM.

PicoGreen® DNA quantification (Quant-iT Picogreen, P7589, Invitrogen) was used to measure the DNA content of the samples incubated with ADSCs for cellular adherence and proliferation. After 6h, 1, 3, and 7 days incubation, Cells were lysed with 1% triton X-100 and subjected to several freeze-thaw cycles. From the lysates (25 µL), DNA content was calculated using PicoGreen® DNA quantification (Quant-iT Picogreen, P7589, Invitrogen) according to manufacturer's instructions. Briefly, 75 µL of Picogreen® reagent was incubated with each lysate for 5 minutes, at room temperature, protected from light. Fluorescence of the samples was measured at 485/535 nm using a Victor3 multilabel fluorescence plate reader (PerkinElmer, USA). Samples were assayed at 6 hours, 1, 3 and 7 days and the DNA content determined with reference to a standard curve. The cell number were converted from DNA values and plotted.

3.5 Statistical Analysis

Data were expressed as the mean ± standard deviation. Statistical analyses were performed using the t-test. All data were analyzed with SPSS software (version 11.0).

4. Conclusion

In the present study, we developed a novel method for fabrication of graphene composite nanofiber mats, which demonstrated that graphene could be fabricated into fine size nanofibers (diameter < 500nm) with uniform and smooth surface. The produced rGO-NFMs have presented superior mechanical properties and outstanding electrical properties. ADSCs as model cells were cultured on the rGO-NFMs to test its effect on the cell proliferation and morphology. The results showed that cells could form interated cell-nanofiber constructs after 3 day in culture, and DNA assay confirmed that the attachment and proliferation of ADSCs cultured on rGO-NFMs are similar to that of PAN-NFMs and TCPs. These results demonstrated that the rGO-NFMs will have great prospects in the field of tissue engineering.

Acknowledgements

We acknowledge the financial support by the National Natural Science Foundation of China (Grant No: 21171179), the project of Scientific Research Innovation Foundation of Zhoukou Normal University (Grant No:zknuA201406), High Level Personnel Fund of Zhoukou Normal University (ZKNUB2013007), the project of Innovation Scientists and Technicians Troop Construction Projects of Henan Province

(No:2013259), the project of Henan Province Key Discipline of Applied Chemistry (No:201218692), the program of Innovative Research Team (in Science and Technology) in University of Henan Province (14IRTSTHN009) and Key Science and Technology Program of Henan Province (132102310491).

Notes and references

^aThe Key Laboratory of Rare Earth Functional Materials and Applications, Zhoukou Normal University, Zhoukou 466001, P. R. China

¹⁰ Fax&Tel: +86-394-8178518.

Email: jinlin_1982@126.com; zlwang2007@hotmail.com

^bDepartment of Oral and Maxillofacial Surgery, Guanghua School of Stomatology, Hospital of Stomatology, Guangdong Provincial Key Laboratory of Stomatology, Sun Yat-Sen University, Guangzhou 510055, P. R. China

^cDepartment of Prosthodontics, Guanghua School of Stomatology, Hospital of Stomatology, Sun Yat-Sen University, Guangzhou 510055, P. R. China

^dSchool of Mechanical and Aerospace Engineering, Nanyang

²⁰ Technological University, 639798, Singapore

^eInstitute for Micromanufacturing, Louisiana Tech University, 911

Hergot Ave., Ruston LA 71272, USA

1 Z. P. Chen, W. C. Ren, L. B. Gao and H. M. Chen, *Nat. Mater.*, 2011, **10**, 424-428.

²⁵ X. B. Cao, D. P. Qi, S. Y. Yin, J. Bu, F. J. Li, C. F. Goh, S. Zhang and X. D. Chen, *Adv. Mater.*, 2013, **25**, 2957-2962.

3 L. L. Liu, Z. Q. Niu, L. Zhang, W. Y. Zhou, X. D. Chen and S. S. Xie, *Adv. Mater.*, 2014, doi:10.1002/adma.201401513.

4 D. B. Kong, H. Y. He, Q. Song, B. Wang, Q. H. Yang and L. J. Zhi, *RSC Adv.*, 2014, **4**, 23372-23376.

³⁰ K. K. Purushothaman, B. Saravanakumar, I. M. Babu, B. Sethuraman and G. Muralidharan, *RSC Adv.*, 2014, **4**, 23485-23491.

6 O. K. Park, M. G. Hahn, S. Lee, H. I. Joh, S. I. Na, J. H. Lee, B. C. Ku, and P. M. Ajayan, *Nano Lett.*, 2012, **12**, 1789-1793.

³⁵ 7 Y. Q. Li, T. Yu and T. Y. Yang, *Adv. Mater.*, 2012, **24**, 3426-3431.

8 T. Kuila, S. Bose, A. K. Mishra, P. Khanra, N. H. Kim and J. H. Lee, *Prog. Mater. Sci.*, 2012, **57**, 1061-1105.

9 Q. L. Bao, H. Zhang, J. X. Yang, S. Wang, D. Y. Tang, R. Jose, S. Ramakrishna, C. T. Lim and K. P. Loh, *Adv. Funct. Mater.*, 2010, **20**, 782-791.

⁴⁰ 10 S. Shah, P. T. Yin, T. M. Uehara, S. T. D. Chueng, L. T. Yang and K. B. Lee, *Adv. Mater.*, 2014, **26**, 3673-3680.

11 S. Stankovich, D. A. Dikin, G. H. B. Dommett, K. M. Kohlhaas, E. J. Zimney, E. A. Stach, R. D. Piner, S. T. Nguyen and R. S. Ruoff, *Nature*, 2006, **442**, 282-286.

12 R. Verdejo, F. Barroso-Bujans, M. A. Rodriguez-Perez, J. A. D. Saia and M. A. Lopez-Manchado, *J. Mater. Chem.*, 2008, **18**, 2221-2226.

13 A. Yu, P. Ramesh, M. E. Itkis, E. Bekyarova and R. C. Haddon, *J. Phys. Chem. C*, 2007, **111**, 7565-7569.

⁵⁰ 14 N. Liu, F. Luo, H. Wu, Y. H. Liu, C. Zhang and J. Chen, *Adv. Funct. Mater.*, 2008, **18**, 1518-1525.

15 T. Ramanathan, A. A. Abdala, S. Stankovich, D. A. Dikin, M. Herrera Alonso, R. D. Piner, D. H. Adamson, H. C. Schniepp, X. Chen, R. S. Ruoff, S. T. Nguyen, I. A. Aksay, R. K. Proud'homme and L. C. Brinson, *Nat. Nanotechnol.*, 2008, **3**, 327-331.

⁵⁵ 16 G. Eda and M. Chhowala, *Nano Lett.*, 2009, **9**, 814-818.

17 S. D. Wu, W. Lv, J. Xu, D. Han, X. Chen, P. Wang and Q. H. Yang, *J. Mater. Chem.*, 2012, **22**, 17204-17209.

⁶⁰ 18 S. Myung, A. Solanki, C. Kim, J. Park, S. S. Kim and K. B. Lee, *Adv. Mater.*, 2011, **23**, 2221-2225.

19 H. L. Fan, L. L. Wang, K. K. Zhao, N. Li, Z. Shi, Z. Ge and Z. Jin, *Biomacromolecules*, 2010, **11**, 2345-2351.

20 S. Y. Park, J. Park, S. H. Sim, M. G. Sung, K. S. Kim, B. H. Hong and S. H. Hong, *Adv. Mater.*, 2011, **23**, H263-H267.

⁶⁵ 21 K. Zhou, G. A. Thouas, C. C. Bernaerd, D. R. Nisbet, D. I. Finkelstein, D. Li and J. S. Forsythe, *ACS Appl. Mater. Interfaces*, 2012, **4**, 4524-4531.

22 D. Li, M. B. Mller, S. Gilje, R. B. Kaner and G. G. Wallace, *Nat. Nanotechnol.*, 2008, **3**, 101-105.

⁷⁰ 23 Q. Wu, Y. X. Xu, Z. Y. Yao, A. Liu and G. Q. Shi, *ACS Nano*, 2010, **4**, 1963-1970.

24 H. Y. Sun, Z. Xu and C. Gao, *Adv. Mater.*, 2013, **25**, 2554-2560.

25 L. Jin, T. Wang, M. L. Zhu, M. K. Leach, Y. I. Naim, J. M. Corey, Z. Q. Feng and Q. Jiang, *J. Biomed. Nanotechnol.*, 2012, **8**, 1-9.

⁷⁵ 26 L. Jin, Z. Q. Feng, M. L. Zhu, T. Wang, M. K. Leach and Q. Jiang, *J. Biomed. Nanotechnol.*, 2012, **8**, 779-785.

27 L. Jin, T. Wang, Z. Q. Feng, M. K. Leach, J. H. Wu, S. J. Mo and Q. Jiang, *J. Mater. Chem. B*, 2013, **1**, 1818-1825.

⁸⁰ 28 L. Jin, T. Wang, Z. Q. Feng, M. L. Zhu, M. K. Leach, Y. I. Naim and Q. Jiang, *J. Mater. Chem. B*, 2012, **22**, 18321-18326.

29 S. J. Park, J. A. Inhwa, R. D. Piner, S. J. An, X. S. Li, A. Velamakanni and R. S. Ruoff, *Nano Lett.*, 2009, **9**, 1593-1597.

30 Y. Q. Li, T. Yu, T. Y. Yang, L. X. Zheng and K. Liao, *Adv. Mater.*, 2012, **24**, 3426-3431.

⁸⁵ 31 I. Y. Jeon, Y. R. Shin, G. J. Sohn, H. J. Choi, S. Y. Bae, J. Mahmood, S. M. Jung, J. M. Seo, M. J. Kim, D. W. Chang, L. M. Dai and J. B. Baek, *Proc. Natl. Acad. Sci. U. S. A.*, 2012, **109**, 5588-5593.

32 H. J. Salavagione and G. Martinez, *Macromolecules*, 2011, **44**, 2685-2692.

⁹⁰ 33 A. S. Rowlands and J. J. Cooper-White, *Biomaterials*, 2008, **29**, 4510-4520.

34 W. S. Hummers and R. E. Offeman, *J. Am. Chem. Soc.*, 1958, **80**, 1339-1339.

⁹⁵ 35 C. F. Brunk, K. C. Jones and T. W. James, *Anal. Biochem.*, 1979, **92**, 497-500.